LAWRENCE
LIVERMORE
NATIONAL
LABORATORY

LLNL-JRNL-659154

Hydrogen Accumulates in and UH3 Precipitates at U-C-N-O Inclusions in Uranium - a SIMS Analysis

W. J. Siekhaus, P. Weber, I. D. Hutcheon , J. Matzel, W. McLean

August 25, 2014

Journal of Alloys and Compounds

Disclaimer

Hydrogen Accumulation in and at the Perimeter of U-C-N-O Inclusions in Uranium – a SIMS Analysis.

W. J. Siekhaus, P.K. Weber, I.D. Hutcheon, J.E.P. Matzel, W. McLean
Lawrence Livermore National Laboratory, Livermore, CA 94551, USA
Prepared by LLNL under Contract DE-AC52-07NA27344

Abstract

We use imaging secondary ion mass spectrometry (SIMS) with a Cameca NanoSIMS 50 to determine the distribution and relative concentration of H in two uranium metal samples [sample1(LANL) as cast with less than 1wppm H, sample2(Y12), outgassed 6 hours in vacuum at 630C to remove hydrogen}. H ion counts appear almost exclusively associated with 'carbide' inclusions, based on H^-, C^- and O^- ion images for uranium surfaces sputter-cleaned in situ with a 16keV Cs^+ ion beam. Two classes of inclusions are identified: small, micrometer to sub-micrometer inclusions and larger, clearly angular inclusion (≥ 3μm). In sample1(LANL) the large inclusions (≥ 250/mm^2) show a low H^-/C^- ratio inside, and have H^-/C^- ratios at their perimeters comparable in magnitude to that seen in μm-size inclusions. Small inclusions (~ 2500/mm^2) contain H more uniformly throughout and, averaged over the inclusion, the small inclusions have approximately 50 times higher relative H concentration than the large inclusions. Sample2(Y12) was found to have comparable H^-/C^- ratios in the large carbides, but no small inclusions were observed. Because of the matrix-sensitivity of SIMS, H/C ratios representing the actual composition of the inclusions cannot be derived from the H^-/C^- ratios without calibration UC samples with known H content, which are not currently available.

1. Introduction

Uranium metal typically contains many precipitates of impurities above their solubility limits [1], among them UH_3. The spatial distribution of carbides, nitrides, oxides is easily seen on surfaces by optical or SEM microscopy, but the distribution of UH_3 is not easily identifiable, unless the surface is prepared and observed in a specific manner[2] where electrochemical treatment produces a product of distinctive color from hydride inclusions, or in an inert environment, e.g., by in-situ sputtering in ultra-high vacuum, since UH_3 is pyrophoric and will convert to uranium oxide. Its existence in uranium super-saturated in hydrogen is, however, clear from the H-U phase diagram[3]. Also, small angle neutron scattering (SANS) experiments[4, 5] indicate inclusions of high hydrogen content in uranium that has hydrogen content substantially above the hydrogen solubility limit (14 wppm). SANS does, however, not prove that those inclusions are UH_3. Hydrogen's spatial distribution may affect uranium's mechanical properties[2]. It may lead to localized surface hydriding if the oxide layer that usually covers uranium metal is defective above a hydride inclusion, as is suggested as a possibility in [6]. UH_3 exposed to an oxygen-containing environment during surface preparation will, in contrast to oxide formed on the metal itself, produce an oxide with simultaneous evolution of hydrogen, and hence may be defective.. We find a strong correlation between hydrogen and uranium carbide inclusions, with high concentration of hydrogen in μm-size inclusions and on the perimeter of above-μm-size carbides. That finding is consistent with Beevers's [2] interpretation of Davis's[7] work on hydrogen in uranium "..0-0.2

ppm, hydrogen was absorbed by uranium carbide and other precipitates; 0.2-0.4 ppm, hydrogen was taken into solution by the uranium metal and 0.4-2.0 ppm; uranium hydride precipitates were formed." (Davis' ppm refers to mass ratio, which we refer to as wppm). Cracks may appear during thermal treatment associated with hydriding experiments[8, 9] in the oxide formed there from material of high hydrogen content since the thermal expansion coefficients of uranium carbides differ from that of uranium metal[10-13].

2. Materials and Methods

Two samples were used. For sample1(LANL), uranium rods of approximately 6 mm diameter were cast at Los Alamos National Laboratory[14] with a typical impurity content, i.e., density of large inclusions of about 355/mm^2 and a hydrogen content of less than 1.0 wppm (weight of H/weight of U238), and a sample of approximately 1.5 mm thickness was cut using EDM (electrical discharge machining). For sample2(Y12) (machined to 12.7 mm diameter, 6.35 mm thick) rods were cast at Y12, subsequently heated in ultra high vacuum at ~630°C for six hours to reduce its hydrogen content from its original content (0.45±0.149 wppm)[15] by more than a factor 100[16] to $\leq$ 0.01 wppm and then quenched in water They were ground with SiC grinding paper to 800 grit using water as lubricant and then polished using first 3 micron and finally 1 micron diamond suspension, 15N force, with propylene glycol lubricant, rinsed with alcohol, and stored in 10^{-4} Pa vacuum. Imaging secondary ion mass spectroscopy (SIMS) was performed with the LLNL NanoSIMS 50 (Cameca, Geneviers, France). Both samples were introduced into the NanoSIMS, and square areas (1600 to 12600 μm^2) were sputtered in situ to depths between 0.5 μm and 9 μm using 1 nA of 16 keV Cs^+ ions. Secondary electron (e^-) and ion images of H^-, C^- and O^- were acquired using 16 keV Cs^+ ions with currents between 3 and 15 pA, with a lateral resolution of about 200 nm, as can be seen in Fig. 2. The sputtering-induced Cs content of the surface decreases the surface's work function and facilitates negative ion emission of non-metallic constituents. Negative metal ions, such as (U^-) are rarely generated; hence we did not establish a H/U. Neither did we establish an absolute elemental H/C ratio as it exist in the material, since the ion yield in SIMS is matrix-sensitive, and U-C-H standards of known compositions are not available.

3. Results

Figure 1 shows the NanoSIMS H^-, e^-, C^-, and O^- images (labeled 'a', 'b', 'c', 'd', respectively) of a 90 x 90 μm^2 region of U metal of sample1(LANL) after sputtering to a depth of 4.8μm. The $^{12}C^-$ image ('c') shows two large UC_x inclusions and the distribution of small inclusions. We define "large inclusions" as angular inclusions that are easily visible in optical micrographs and have diameters 'above several μm' (the ones in figure 1 have above 5μm diameter), and "small inclusions" to have micrometer to sub-micrometer diameter, difficult to detect in optical micrographs. The a:)H^- and c:)C^- images demonstrate for both inclusion sizes a high correlation of H^- and C^- intensities.

Scaling in the images is set to above saturation for some regions to make the correlation easier to see. The secondary electron image b:)e^- shows sample morphology. O^- [image d:)] appears at the edge of only one of the large UC_x inclusions, but its count rate intensity is not correlated with H^- and C^- in the small inclusions. Six such areas were analyzed, and Table 1 demonstrates that the number density of small inclusions containing both C and H varies greatly, from zero to 123.5 per 10^4 μm^2, with an average of ~ 27 per 10^4 μm^2. Figure 2 displays H^-, C^-, and O^- counts along line sections through inclusions in sample1(LANL). Picture 'b' is a transect through the large inclusion whose H- image is picture 'a'. Pictures 'c', 'd' and 'e' are transects through the three smaller inclusions in picture 'a'. Because SIMS is matrix-sensitive, changes in count rates as a function of distance along the section are not necessarily the same as changes in actual composition. The H^- counts in picture 'b" is small in the interior of the large inclusion (10.2±3.5 between 4 and 8 μm), but increases substantially at the perimeter (to 51.5 at x=3 and 37.9 at x=9). Several large inclusions were analyzed, and the highest H^- counts occurred at such a perimeter. The highest H^- count values in sections c, d, e, through small inclusions are 25, 21, 30, respectively, comparable to the magnitude of the H^- counts at the perimeter of large inclusions. All three sections in the lower half of Fig. 2 thus exhibit higher H^-/C^- ratios than seen in the inside of large inclusions. Figure 3 summarizes all H^-/C^- ratio measurements of sample1(LANL), as averaged over multiple analysis cycles for both large and small inclusions. Table 2 shows a statistical analysis of those values. That analysis reveals that the average H^-/C^- ratio of large inclusions is about a factor 50 lower than the average H^-/C^- ratio at small inclusions. The O^- counts are low but detectable in all sections.

Figure 4 depicts a): SE(=secondary electron), b): $1H^-$, c): $12C^-$, d): $14N12C^-$, e): H^- and C^- counts along a section, f): $16O^-$, images, respectively, of the uranium sample2(Y12) outgassed at 630°C for 6hr, reducing its initial hydrogen content of 0.45±0.149 wppm by more than a factor 100 to ≤ 0.0045 wppm, assuming the hydrogen diffusion coefficient of [16]. Average hydrogen content in the large inclusions is comparable to sample1(LANL) (~0.01 H^-/C^-). However, the H^-/C^- ratio at the perimeter of these carbide inclusions is much lower than in sample1(LANL) (0.1 vs. ~1), and no small H and C inclusions comparable to sample1(LANL) were detected in four 3600μm^2 areas analyzed. Figure 4 demonstrates furthermore, that large inclusions contain H^-, C^-, O^- and N^-, thus are NOT pure uranium carbides, or uranium oxides, or uranium nitrides, but rather an agglomeration or co-precipitation.

4. Discussion

As pointed out before, SIMS is highly 'matrix-dependent' and hence cannot establish absolute ratios of elemental content without a calibration standard with elemental composition comparable to that of the inclusions analyzed here. Hence it is possible that secondary ion emission probability (a.k.a., ion yield) and hence the measured count rate of any constituent may be affected at the transition from uranium metal to inclusion.

However, we can expect that ion yields will be sufficiently constant for similar phases, such as U_xC_y, to allow ion ratios to be used to make defensible comparisons of 'relative concentrations'. The ion ratios as we record them suggest (see Figures 1 and 2): a) in uranium hydrogen preferentially accumulates at carbon-containing inclusions, confirming a sixty year old suggestion [6], b) the interior of 'large' 'carbide' inclusions has a significant lower H^-/C^- ratio than that found at their perimeter or at 'small' carbide inclusions. Figure 4 confirms: c:) 'carbide' inclusions are really an agglomerate of oxide, nitride, and carbide precipitates; but carbon has the highest concentration[1], and hence these inclusions are often labeled 'carbides'.

The observation listed under a) is consistent with Beevers' summary of Davis' observations (quoted above)[2]; the H background in SIMS is typically too high to accurately detect the very low concentration of hydrogen in uranium metal itself at room temperature. To b) the observed low relative H concentration (i.e., H^-/C^- ratio) inside large inclusions and the higher relative concentration at their perimeter: Uranium is heated and held for some time in low quality vacuum above its melting point in carbon crucibles and then cast into carbon forms. Since the melting points of uranium carbides, nitrides and oxides are substantially above the melting point of uranium metal, large inclusions can be formed in the melt since the diffusion coefficient for all impurities is high at that temperature. Some of these inclusions stay in the melt despite their lower density because of eddy currents induced by the heating technique. Uranium hydride, however, can only form at low temperature[3]. The hydrogen content seen inside 'large' 'carbide' inclusions may hence be in equilibrium with the hydrogen content in uranium while it is liquid. The solubility of hydrogen in UC and the ternary UCH phase diagram are not known, but the ternary phase diagrams of lanthanide-carbon-hydrogen compounds [17, 18] showing $YbC_{0.5}H$ and $YbCH_{0.5}$, $La_2C_{3-x}H_{1.5\_x}$, La_2CH_4, $La_2C_2H_2$ phases suggest that uranium carbide may also be able to accommodate hydrogen. The solubility of all impurities and their diffusivity in uranium decreases with decreasing temperature, including hydrogen's [16], and hence only smaller 'carbide' precipitates can form during the cool-down. Hydrogen in the metal above the decreasing solubility limit will diffuse to and aggregate at the boundaries of existing large inclusions as well as at small carbide inclusions as they precipitate. The fact that comparable relative H concentration is found at the perimeter of large inclusions and in small inclusions may reflect the hydrogen content of the limited range from which hydrogen can diffuse during the cool-down. This hypothesis is further supported by the results of extended heating under ultra high vacuum. Relative H concentration was reduced in the perimeter of carbide inclusions, while the relative H concentration in the interior of large carbides was not substantially affected. No small carbide inclusions were found in sample2Y12 in the four 3600μm^2 areas analyzed. The diffusion coefficient of carbon in uranium[19] predicts a diffusion distance $d=\sqrt{(D*t)}$ of 0.0465 cm for a sample held at 630C for 6 hr. The density of large inclusions for Y12 samples[14] is between 375 and 661 per mm^2, with an average distance between large inclusions between 0.053 to 0.039 cm. Hence small carbides can disappear through carbon diffusion to and Oswald ripening of larger inclusions. The thermal expansion coefficients of uranium metal and of the constituents of the 'carbide' precipitates differ [10-12, 20], and hence the crystal structure at the boundary will be unstable during cool-down and capable of accommodating hydrogen.

The presence of UH_3 at 'carbide' boundaries was postulated as a possible cause of the spot-wise hydride formation at uranium surfaces [6]. Arkush [21] found hydride attack preferentially at the edge of large (>3μm) 'carbide' inclusions where we find the highest relative H concentration. A more recent uranium hydriding study[22] did, under the particular conditions the hydride was formed, find "that the hydride growth sites on the sample surface were almost exclusively coincident with exposed carbo-nitride phases", but their SIMS analysis, using a Ga+ ion beam and analyzing both positive and negative secondary ions, did not detect H^- ions either in or at the perimeter of said inclusions, and attributed the preferential hydriding attack to other factors at the perimeter. Indeed, the oxide formed from UH_3 may be different from the oxide formed on uranium metal, may include hydrogen and lack the strength and the protective property of uranium oxide formed on the metal itself.

5. Conclusions.

SIMS analysis of sputter-cleaned surfaces of impure uranium using Cs^+ ions clearly shows H^- strongly correlated to C^-. H^- counts appear inside of and, at much higher observed intensity, at the boundary of large (i.e., larger than a few micrometer) inclusions and about that same high intensity inside small 'carbide' precipitates of sample1(LANL). We did not find small carbide precipitates in sample2(Y12) after outgassing it in vacuum at 630C for six hours; the relative H concentration was reduced at the perimeter of large carbide inclusions, while the relative H concentration in the interior of large carbides was not substantially affected. SIMS cannot prove that hydrogen is present as UH_3, since negative U- metal ions are not generated. SIMS does identify 'carbide' precipitates in uranium as an agglomeration of uranium compounds with carbon, nitrogen and oxygen.

5. Figure Captions

Figure 1. a, c, and d): NanoSIMS H^-, C^-, and O^- images, respectively, of a 90 x 90 μm^2 region of sample1(LANL), with two large and a number of small inclusions. They demonstrate the strong correlation between H^- and C^- ion counts in the SIMS elemental images. b): secondary electron emission image of the same area. Table 1 shows that the number density of small inclusions shown in images 'a' and 'c' producing both C^- and H^- varies greatly, from zero to 123.5 per 10^4 μm^2, with an average number density N of ~ 27 per 10^4 μm^2 = ~ 2700/mm^2.

Figure 2. a): H^- image of a large inclusion. b): H^-, C^- and H^-/C^- counts along the dotted yellow section line in a). c, d and e): H^-, C^- and H^-/C^- counts, respectively, along sections through the three small inclusions in a).

Figure 3. H^-/C^- ratios, averaged over the whole sample, for all small and large inclusions analyzed. The H^-/C^- ratio is based on actual counts, since a calibration sample with known concentrations of U, C, and H is not available.

Figure 4. a): SE(=secondary electron), b): $1H^-$, c): $12C^-$, d): $14N12C^-$, e): H^-, C^-, and H^-/C^- counts along a section through the inclusion, f): $16O^-$, images, respectively, of the uranium sample2(Y12) outgassed at 630°C for 6hr, reducing its initial hydrogen content of 0.45±0.149 wppm by more than a factor 100 to ≤ 0.0045 wppm, based on the hydrogen diffusion coefficient of [16].

6. Figures

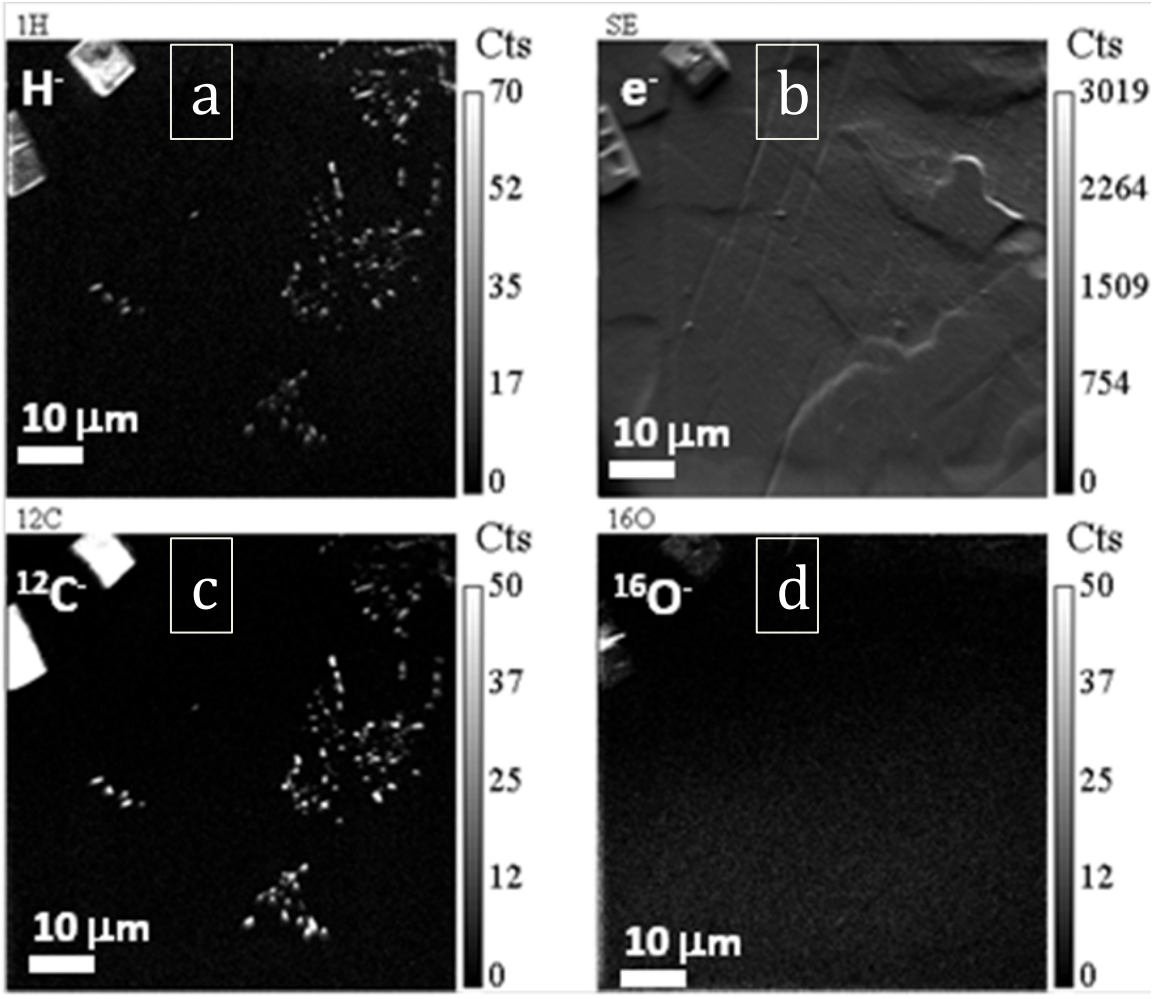

Figure 1.

Figure 2.

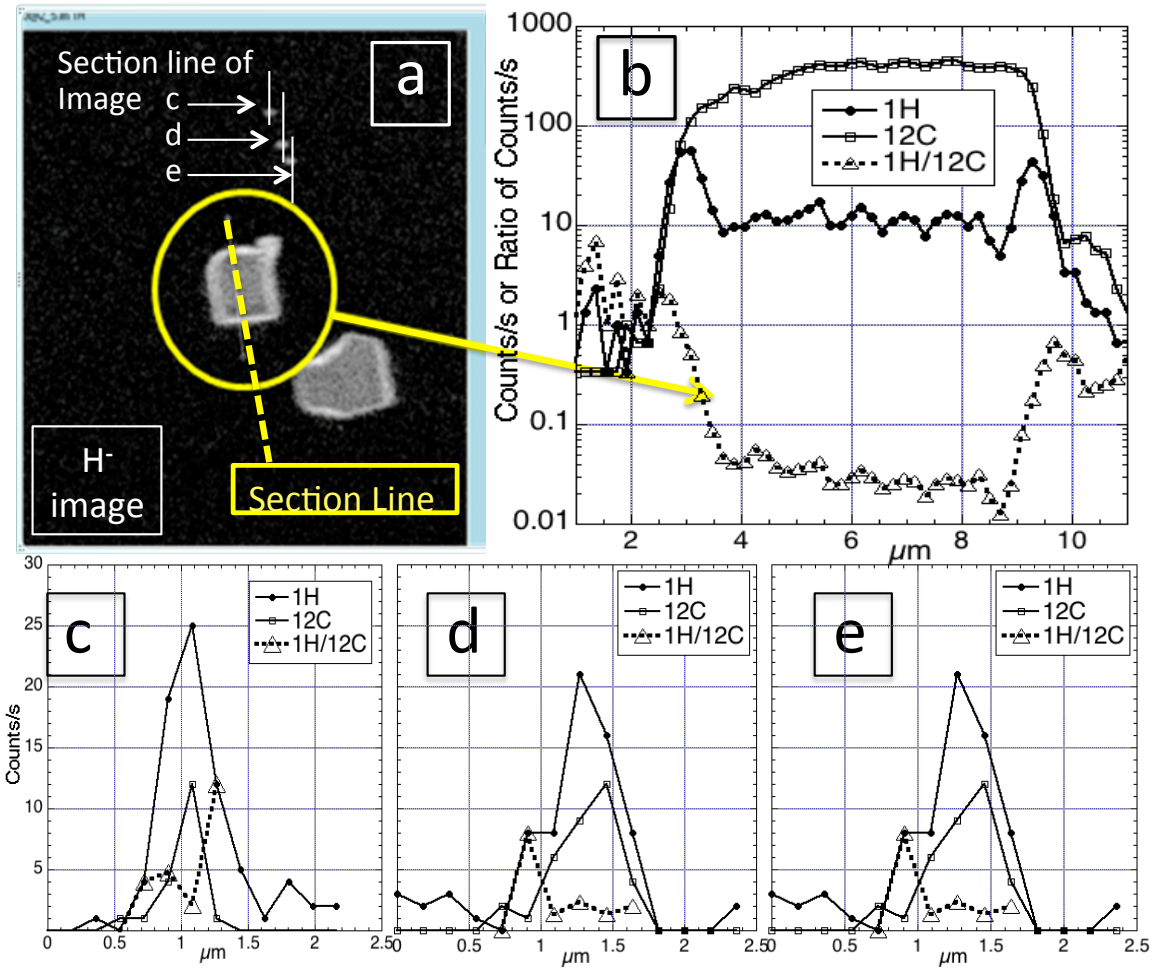
Section line of Image
c
d
e
a
H- image
Section Line
b
1H
12C
1H/12C
Counts/s or Ratio of Counts/s
1000
100
10
1
0.1
0.01
2
4
6
8
10
μm
c
d
e
Counts/s
30
25
20
15
10
5
0
0.5
1
1.5
2
2.5
μm

Figure 3

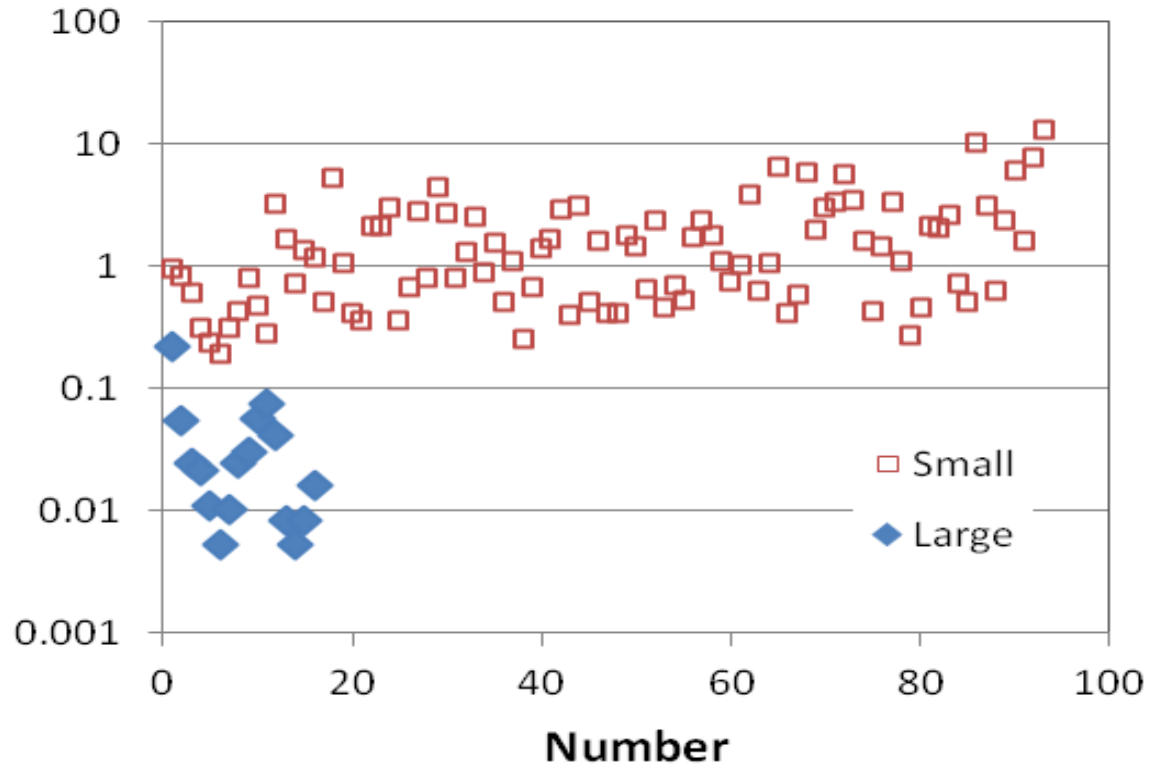

Figure 4.

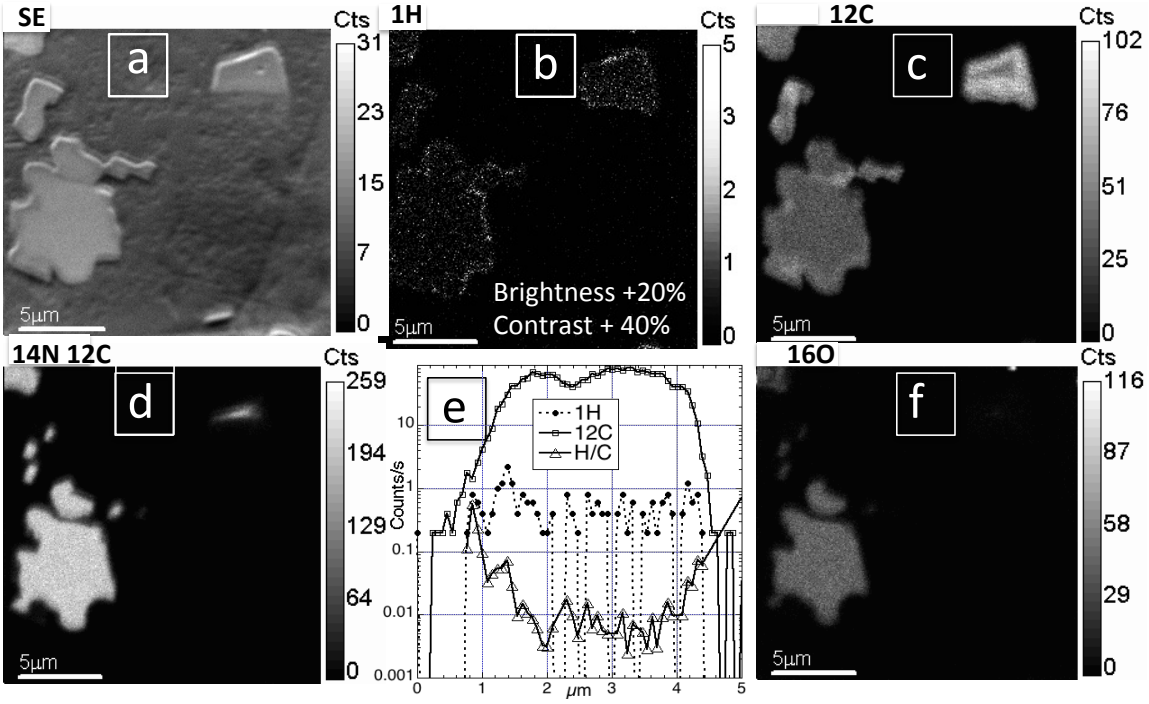
SE
a
Cts
31
23
15
7
0
5µm
1H
b
Cts
5
3
2
1
0
Brightness +20%
Contrast + 40%
5µm
12C
c
Cts
102
76
51
25
0
5µm
14N 12C
d
Cts
259
194
129
64
0
5µm
e
1H
12C
H/C
Counts/s
10
1
0.1
0.01
0.001
0
1
2
µm
3
4
5
16O
f
Cts
116
87
58
29
0
5µm

Tables

Table 1.

Area #	Analysis Current (pA)	Analysis raster (μm)	Number of small inclusions		Density N of small inclusions ($N/10^4$ μm^2)
A6	3	90	2		2.5
A7	15	90	100		123.5
A8	15	90	11		13.6
A10	15	90	7		8.6
A12	15	50	0		0
A13	15	50	3		12
				Median	10.3
				Average	26.7
				Weighed average	32.9
				Number of areas	6

Table 1.
Statistics of the number of small inclusions in six areas of sample1(LANL)

Table 2.

	Median $^1H^-/^{12}C^-$	Average $^1H^-/^{12}C^-$	SD	SE	N
Large inclusions	0.023	0.038	0.053	0.013	16
Small inclusions	1.10	1.87	2.09	0.22	93

Table 2. H^- to C^- ion ratio statistics for large and small inclusions in image 'a' of Fig. 3.
SD = standard deviation; SE = standard error; N = number of analyses

7. References

[1] G.L. Powell, J.B. Condon, Mass Spectrographic Determination of Hydrogen Thermally Evolved from Uranium and Uranium Alloys, Analytical Chemistry, 45 (1973) 2349-2354.
[2] C.J. Beevers, G.T. Newman, Hydrogen Embrittlement in Uranium, J Nucl Mater, 23 (1967) 10-18.
[3] T.R. Massalski, Binary Alloy Phase Diagrams, American Society For Metals, Metals Park, Ohio 44073, 1986.
[4] S. Spooner, G.M. Ludtka, J.S. Bullock, R.L. Bridges, G.L. Powell, J. Barker, SANS measurement of Hydrides in Uranium, in, Y-12 National Security Complex, Y/DZ-2346, Oak Ridge, TN, 2001, pp. 12.
[5] S. Spooner, J.S. Bullock, R.L. Bridges, G.L. Powell, G.M. Ludtka, J. Barker, SANS measurement of hydrides in uranium, in: N.R. Moody, A.W. Thompson, R.E. Ricker, e. al. (Eds.) Hydrogen Effects on Material Behavior and Corrosion Deformation Interactions, Joint TMS/ASM Environ. Effects Committee, Structural Mater. Div. (SMD) of TMS (The Minerals, Metals & Mater. Soc.); Environ. Sensitive Fracture Working Group, European Federation of Corrosion; Nat. Inst. of Standards and Technol.; Sandia Nat. Lab, Moody, N.R.; Thompson, A.W.; Ricker, R.E.; et al., 2002, pp. 269-278.
[6] L.W. Owen, R.A. Scudamore, A Microscope Study of Initiation of Hydrogen-Uranium Reaction, Corrosion Science, 6 (1966) 461-468.
[7] W.D. Davis, Solubility, Determination, Diffusion and Mechanical Effects of Hydrogen in Uranium, in, Knolls Atomic Power Laboratory, KAP-1548, 1956.
[8] S.G. Bazley, J.R. Petherbridge, J. Glascott, The influence of hydrogen pressure and reaction temperature on the initiation of uranium hydride sites, Solid State Ionics, 211 (2012) 1-4.
[9] J.P. Knowles, I.M. Findlay, D.A. Geeson, S.G. Bazley, The Influence of Vacuum Annealing on the Nucleation and Growth Kinetics of Uranium Hydride, Actinides and Nuclear Energy Materials, 1444 (2012) 211-216.
[10] R. Mendezpenalosa, R.E. Taylor, Thermal Expansion of Uranium Monocarbide, J Am Ceram Soc, 47 (1964) 101-102.
[11] S. Ihara, M. Suzuki, Y. Akimoto, High-Temperature Thermal Lattice Expansion of Mixed Carbo-Nitride and Uranium Carbo-Nitride, J Nucl Mater, 39 (1971) 311-&.
[12] A.L. Bowman, G.P. Arnold, W.G. Witteman, T.C. Wallace, Thermal Expansion of Uranium Dicarbide and Uranium Sesquicarbide, J Nucl Mater, 19 (1966) 111-&.
[13] L.T. Lloyd, Thermal Expansion of Alpha-Uranium Single Crystals, J Nucl Mater, 3 (1961) 67-71.
[14] R.K. Schulze, M.A. Hill, Parametric Study for Hydrogen Reactivity of Engineered Uranium Surfaces, in, Las Alamos National Laboratory, LA-UR-08-1879, 2008.
[15] E. Garlea, J.S. Morrell, G.L. Powell, R.L. Bridges, Effects of Hydrogen on Mechanical Properties of Cast Uranium, in, Y-12 National Security Complex, Y/DZ-3075, Oak Ridge, Tennessee, 2010.
[16] G.L. Powell, Hydrogen in Uranium, in, Y12 National Security Complex, Y/DZ-2797, Oak Ridge, Tennessee, 2007.

[17] J.M. Haschke, Preparation and Some Properties of Ytterbium Carbide Hydrides, Inorg Chem, 14 (1975) 779-783.
[18] A. Simon, T. Gulden, La2C3 and its reaction with hydrogen, Z Anorg Allg Chem, 630 (2004) 2191-2198.
[19] F.A. Schmidt, O.N. Carlson, Electrotransport of Carbon in Molybdenum and Uranium, Metall Trans A, 7 (1976) 127-132.
[20] L.T. Lloyd, C.S. Barrett, Thermal Expansion of Alpha Uranium, J Nucl Mater, 18 (1966) 55-59.
[21] R. Arkush, A. Venkert, M. Aizenshtein, S. Zalkind, D. Moreno, M. Brill, M.H. Mintz, N. Shamir, Site related nucleation and growth of hydrides on uranium surfaces blisters, J Alloy Compd, 244 (1996) 197-205.
[22] N.J. Harker, T.B. Scott, C.P. Jones, J.R. Petherbridge, J. Glascott, Altering the hydriding behaviour of uranium metal by induced oxide penetration around carbo-nitride inclusions, Solid State Ionics, 241 (2013) 46-52.